

# Searches for resonances in the $t\bar{b}$ and $t\bar{c}$ final states at the high-luminosity LHC

Elizabeth Drueke,<sup>1</sup> Brad Schoenrock,<sup>1</sup> Barbara Alvarez Gonzalez,<sup>1</sup> and Reinhard Schwienhorst<sup>1</sup>

<sup>1</sup>*Department of Physics and Astronomy,  
Michigan State University, East Lansing MI 48824, USA*

(Dated: April 28, 2019)

## Abstract

We study resonances decaying to one top quark and one additional quark ( $b$  or  $c$ ) at the low-luminosity and high-luminosity 14 TeV LHC and at a future 33 TeV hadron collider in the context of Snowmass 2013. A heavy  $W'$  boson that preferentially couples to quarks can be found through its decay to  $t\bar{b}$ . A Kaluza-Klein gluon might have a significant branching ratio to  $t\bar{c}$ . The final state in these searches has a lepton and neutrino from a  $W$  boson decay plus two jets, at least one of which is  $b$ -tagged. We give expected limits as a function of  $W'$  boson and  $KKg$  masses for different collider energy and integrated luminosity options.

PACS numbers: 14.65.Jk, 14.65.Ha, 12.60.-i, 14.80.Rt

# 1 I. INTRODUCTION

2 The Large Hadron Collider (LHC) is the highest-energy particle accelerator ever built,  
 3 probing physics at the TeV scale. The Higgs boson discovery [1, 2] was the first, but more  
 4 discoveries are likely as the LHC covers the energy range where new physics is expected.  
 5 Searches for high-mass resonances take advantage of the high center-of-mass (CM) energy of  
 6 the LHC and have been performed in many final states. The  $tb$  mode, where  $tb$  corresponds  
 7 to  $t\bar{b}$  and  $\bar{t}b$ , is particularly sensitive to a heavy partner of the  $W$  boson, i.e. a  $W'$  boson  
 8 coupling primarily to quarks and the third generation [3]. Such a  $W'$  boson appears in new  
 9 physics models that have additional symmetries, such as universal extra dimensions [4] or  
 10 little Higgs models [5].

11 Searches for a  $W'$  boson have been performed by ATLAS [6, 7] and CMS [8], with  $W'$  mass  
 12 limits approaching 2 TeV for different  $W'$  couplings. The Feynman diagram for  $W'$  produc-  
 13 tion is shown in Fig. 1. We focus on  $W'$  bosons with purely right-handed couplings, the  
 14 sensitivity to left-handed or mixed couplings is similar.

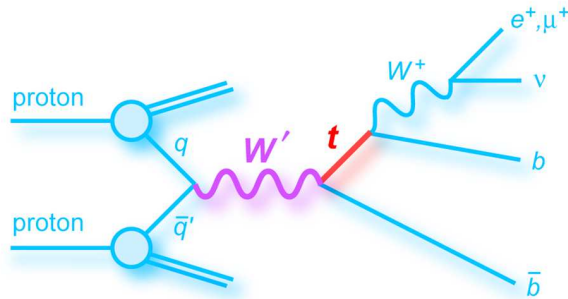


FIG. 1: Feynman diagram for the production of a  $W'$  boson with decay to lepton+jets.

15 Another possibility that has not been explored experimentally yet is the flavor-changing  
 16 neutral current (FCNC) decay of a Kaluza-Klein gluon ( $KKg$ ) [9]. We study a  $KKg$  that  
 17 has a non-negligible branching ratio to  $tc$ , where  $tc$  corresponds to  $t\bar{c}$  and  $\bar{t}c$  [10]. The  
 18 Feynman diagram for  $KKg$  production is shown in Fig. 2. It is likely that such a particle  
 19 will be discovered first in its dominant  $t\bar{t}$  decay mode, and we present the 95% confidence  
 20 level (C.L.) limit as a function of the  $KKg$  mass for the process  $pp \rightarrow KKg \rightarrow tc$ , at a  
 21 cross-section corresponding to a 40% of the  $KKg \rightarrow t\bar{t}$  cross-section [11], which is evaluated  
 22 at next-to-leading order (NLO) in QCD [12] by scaling the leading order (LO) cross section

23 by a factor 1.3.

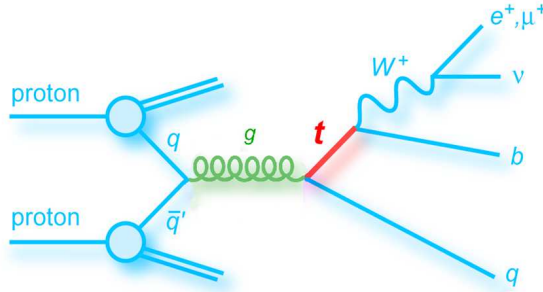


FIG. 2: Feynman diagram for the production of a  $KKg$  with decay to lepton+jets.

24 In this paper we explore the sensitivity of 14 TeV and 33 TeV proton-proton colliders  
 25 to  $W'$  bosons and  $KKg$  in three different scenarios under investigation for the Snowmass  
 26 2013 process:  $300 \text{ fb}^{-1}$  at 14 TeV with an average pileup of 50 events,  $3000 \text{ fb}^{-1}$  at 14 TeV  
 27 with an average pileup of 140 events, and  $3000 \text{ fb}^{-1}$  at 33 TeV with an average pileup of  
 28 140 events. For each scenario the Snowmass LHC detector models are used [13].

29 This paper is organized as follows: Section II introduces the  $W'$  and  $KKg$  models and  
 30 their parameters. Section III explains the event selection. Section IV present the analysis  
 31 strategy. Section V describes the limit setting procedure and shows the results and, finally,  
 32 Section VI gives our conclusions.

## 33 II. SIGNAL AND BACKGROUND MODELING

34 The  $W'$  and  $KKg$  events are generated with Madgraph5 [14] and passed through  
 35 Pythia8 [15] for showering and Delphes3 [16] for detector modeling, using the Snowmass  
 36 settings [13].

37 At each mass point,  $W'$  and  $KKg$  events are generated with equal amounts of top and  
 38 antitop events, 50,000 each. Only  $W$  boson decays to an electron or a muon are included.

39 In addition to these signal samples, background samples generated for Snowmass are  
 40 used [17]. Those samples are diboson,  $W/\gamma/Z$ +Jets,  $t\bar{t}$ ,  $Wt$ ,  $t$ -channel, and  $s$ -channel single  
 41 top. Each background is normalized according to the corresponding sample cross-section.  
 42 The  $W'$  signal samples are normalized to NLO cross-sections [18] as shown in Table I. The  
 43  $KKg \rightarrow t\bar{c}$  samples are normalized to 40% of the corresponding  $KKg \rightarrow t\bar{t}$  cross-section at

44 NLO as shown in Table II.

$W'$ Mass [TeV]	14 TeV		33 TeV	
	$\sigma_{t\bar{t}}$ [pb]	$\sigma_{tb}$ [pb]	$\sigma_{t\bar{t}}$ [pb]	$\sigma_{tb}$ [pb]
1 TeV	9.97E+00	4.68E+00	3.84E+01	2.29E+01
2 TeV	5.14E-01	1.86E-01	3.29E+00	1.62E+00
3 TeV	5.55E-02	1.81E-02	6.65E-01	2.81E-01
4 TeV	7.72E-03	2.62E-03	1.88E-01	7.21E-02
5 TeV	1.37E-03	5.35E-04	6.37E-02	2.26E-02
6 TeV	3.71E-04	1.61E-04	2.40E-02	8.09E-03
7 TeV	1.57E-04	6.99E-05	9.53E-03	3.18E-03
8 TeV			4.00E-03	1.35E-03
9 TeV			1.76E-03	6.09E-04
10 TeV			8.12E-04	2.97E-04
11 TeV			3.95E-04	1.55E-04
12 TeV			2.08E-04	8.71E-05

TABLE I:  $W'$  production cross-section at NLO at 14 TeV and 33 TeV [18].

### 45 III. ANALYSIS

46 Signal and background events are required to pass the following basic selection cuts for  
 47 both  $W'$  and  $KKg$ . Signal-specific cuts are applied in a second step described in Section IV.

$KKg$ Mass [TeV]	14 TeV	33 TeV
1 TeV	9.83E+00	4.43E+01
2 TeV	5.20E-01	3.55E+00
3 TeV	6.55E-02	6.97E-01
4 TeV	1.28E-02	1.99E-01
5 TeV	3.90E-03	6.92E-02
6 TeV	1.42E-03	2.77E-02
7 TeV	6.60E-04	1.24E-02
8 TeV		5.98E-03
9 TeV		3.11E-03
10 TeV		1.72E-03
11 TeV		1.03E-03
12 TeV		8.06E-04

TABLE II:  $KKg \rightarrow tc$  production cross-section at NLO at 14 TeV and 33 TeV.

$$\begin{aligned}
\text{Exactly one lepton (electron or muon) with} & \quad p_T^\ell \geq 25 \text{ GeV}, & |\eta_\ell| \leq 2.5, \\
\text{At least two jets with} & \quad p_T^j \geq 25 \text{ GeV}, & |\eta_j| \leq 2.5, \\
\text{At least one b-tagged jet with} & \quad p_T^j \geq 25 \text{ GeV}, & |\eta_j| \leq 2.5, \\
\text{Missing energy} & \quad \cancel{E}_T > 25 \text{ GeV}
\end{aligned}$$

(1)

48 where  $p_T^\ell$  and  $\eta_\ell$  correspond to the transverse momentum and pseudorapidity of the lepton,  
49 and  $p_T^j$  and  $\eta_j$  are the transverse momentum and pseudorapidity of each jet. Jets are  
50 reconstructed using the Cambridge-Aachen (CA) jet clustering algorithm [19] with a radius

51 parameter of  $R = 0.8$ , ideal for the high- $p_T$  jets and top quark decays associated with our  
 52 signal and backgrounds.

53 Information about the flavor content of jets is obtained by looking for a match within  
 54  $\Delta R = 1.0$  with a  $b$ -tagged anti-kt jet [20] with radius parameter  $R = 0.4$ .

55 All samples are weighted to cross-section times integrated luminosity, including event-  
 56 specific weights:

$$\frac{\text{Luminosity}[\text{fb}^{-1}] \cdot \text{Cross section}[\text{fb}]}{\text{Number of generated events}} \cdot \text{Event weight} . \quad (2)$$

57 Here, the cross-section corresponds to the signal and background cross-sections described  
 58 in II. The  $W'$  and  $KKg$  cross-sections from Tables I and II are multiplied by an additional  
 59 factor of  $\frac{21}{100}$  to account for the  $W$  boson decay branching ratios to  $e$  or  $\mu$ .

60 Tables III and IV give the expected event yields for  $W'$  and  $KKg$  and the backgrounds,  
 61 respectively, for each of the scenarios under consideration. The signal-to-background ratio is  
 62 shown in Table V for the  $W'$  analysis and in Table VI for the  $KKg$  analysis. The dominant  
 63 background for  $300 \text{ fb}^{-1}$  at 14 TeV is  $t\bar{t}$  production, followed by  $W/\gamma/Z$ +jets. For the  
 64  $3000 \text{ fb}^{-1}$  scenarios at both 14 TeV and 33 TeV,  $W/\gamma/Z$ +jets is the dominant background  
 65 followed by  $t\bar{t}$ .

Preselection	14 TeV		33 TeV
	300 $fb^{-1}$	3000 $fb^{-1}$	3000 $fb^{-1}$
Diboson	1.20E+05	6.51E+06	3.75E+07
$W/\gamma/Z$ +Jets	2.39E+06	5.80E+08	5.39E+09
$t\bar{t}$	4.24E+06	2.28E+08	1.59E+09
$Wt$ single top	3.30E+05	1.75E+07	1.14E+08
$t/s$ -channel single top	3.31E+05	2.36E+07	1.17E+08
$W'$ (1 TeV)	3.43E+05	4.51E+06	1.73E+07
$W'$ (2 TeV)	1.66E+04	1.76E+05	1.14E+06
$W'$ (3 TeV)	1.24E+03	1.27E+04	1.53E+05
$W'$ (4 TeV)	1.25E+02	1.30E+03	2.95E+04
$W'$ (5 TeV)	1.79E+01	1.88E+02	7.45E+03
$W'$ (6 TeV)	4.88E+00	5.50E+01	2.26E+03
$W'$ (7 TeV)	2.63E+00	3.41E+01	7.61E+02
$W'$ (8 TeV)			2.87E+02
$W'$ (9 TeV)			1.15E+02
$W'$ (10 TeV)			5.25E+01
$W'$ (11 TeV)			2.47E+01
$W'$ (12 TeV)			1.36E+01

TABLE III: Signal and background event yields after the preselection for various pileup configurations, luminosities, and energy levels for the  $W'$  analysis.

Preselection	14 TeV		33 TeV
	300 $fb^{-1}$	3000 $fb^{-1}$	3000 $fb^{-1}$
Diboson	1.20E+05	6.51E+06	3.75E+07
$W/\gamma/Z$ +Jets	2.39E+06	5.80E+08	5.39E+09
$t\bar{t}$	4.24E+06	2.28E+08	1.59E+09
$Wt$ single top	3.30E+05	1.75E+07	1.14E+08
$t/s$ -channel single top	3.31E+05	2.36E+07	1.17E+08
$KKg$ (1 TeV)	1.60E+05	2.28E+06	9.38E+06
$KKg$ (2 TeV)	8.85E+03	1.03E+05	6.34E+05
$KKg$ (3 TeV)	8.77E+02	1.03E+04	9.45E+04
$KKg$ (4 TeV)	1.52E+02	1.91E+03	2.17E+04
$KKg$ (5 TeV)	4.65E+01	6.20E+02	6.90E+03
$KKg$ (6 TeV)	1.77E+01	2.47E+02	2.71E+03
$KKg$ (7 TeV)	8.44E+00	1.21E+02	1.26E+03
$KKg$ (8 TeV)			6.57E+02
$KKg$ (9 TeV)			3.61E+02
$KKg$ (10 TeV)			2.09E+02
$KKg$ (11 TeV)			1.28E+02
$KKg$ (12 TeV)			8.36E+01

TABLE IV: Signal and background event yields after the preselection for various pileup configurations, luminosities, and energy levels for the  $KKg$  analysis.



Preselection	14 TeV		33 TeV
	$300 \text{ fb}^{-1}$	$3000 \text{ fb}^{-1}$	$3000 \text{ fb}^{-1}$
$W'$ (1 TeV)	4.63E-02	5.25E-03	6.22E-05
$W'$ (2 TeV)	2.24E-03	2.04E-04	4.20E-06
$W'$ (3 TeV)	1.67E-04	1.48E-05	6.27E-07
$W'$ (4 TeV)	1.69E-05	1.51E-06	1.44E-07
$W'$ (5 TeV)	2.42E-06	2.19E-07	4.58E-08
$W'$ (6 TeV)	6.59E-07	6.39E-08	1.80E-08
$W'$ (7 TeV)	3.56E-07	3.96E-08	8.37E-09
$W'$ (8 TeV)			4.36E-09
$W'$ (9 TeV)			2.40E-09
$W'$ (10 TeV)			1.39E-09
$W'$ (11 TeV)			8.51E-10
$W'$ (12 TeV)			5.55E-10

TABLE V: Ratio of signal over background event yields after the preselection for various  $W'$  masses.

Preselection	14 TeV		33 TeV
	$300 \text{ fb}^{-1}$	$3000 \text{ fb}^{-1}$	$3000 \text{ fb}^{-1}$
$KKg$ (1 TeV)	2.16E-02	2.67E-03	1.29E-03
$KKg$ (2 TeV)	1.19E-03	1.20E-04	8.74E-05
$KKg$ (3 TeV)	1.18E-04	1.20E-05	1.30E-05
$KKg$ (4 TeV)	2.05E-05	2.24E-06	3.00E-06
$KKg$ (5 TeV)	6.28E-06	7.25E-07	9.52E-07
$KKg$ (6 TeV)	2.39E-06	2.89E-07	3.74E-07
$KKg$ (7 TeV)	1.14E-06	1.42E-07	1.74E-07
$KKg$ (8 TeV)			9.06E-08
$KKg$ (9 TeV)			4.98E-08
$KKg$ (10 TeV)			2.89E-08
$KKg$ (11 TeV)			1.77E-08
$KKg$ (12 TeV)			1.15E-08

TABLE VI: Ratio of signal over background event yields after the preselection for various  $KKg$  masses.

66 Figures 4 and 3 show kinematic distributions for these preselection variables when cuts  
67 are applied in the order given in Eq. 1, for  $KKg$  and  $W'$ , respectively.

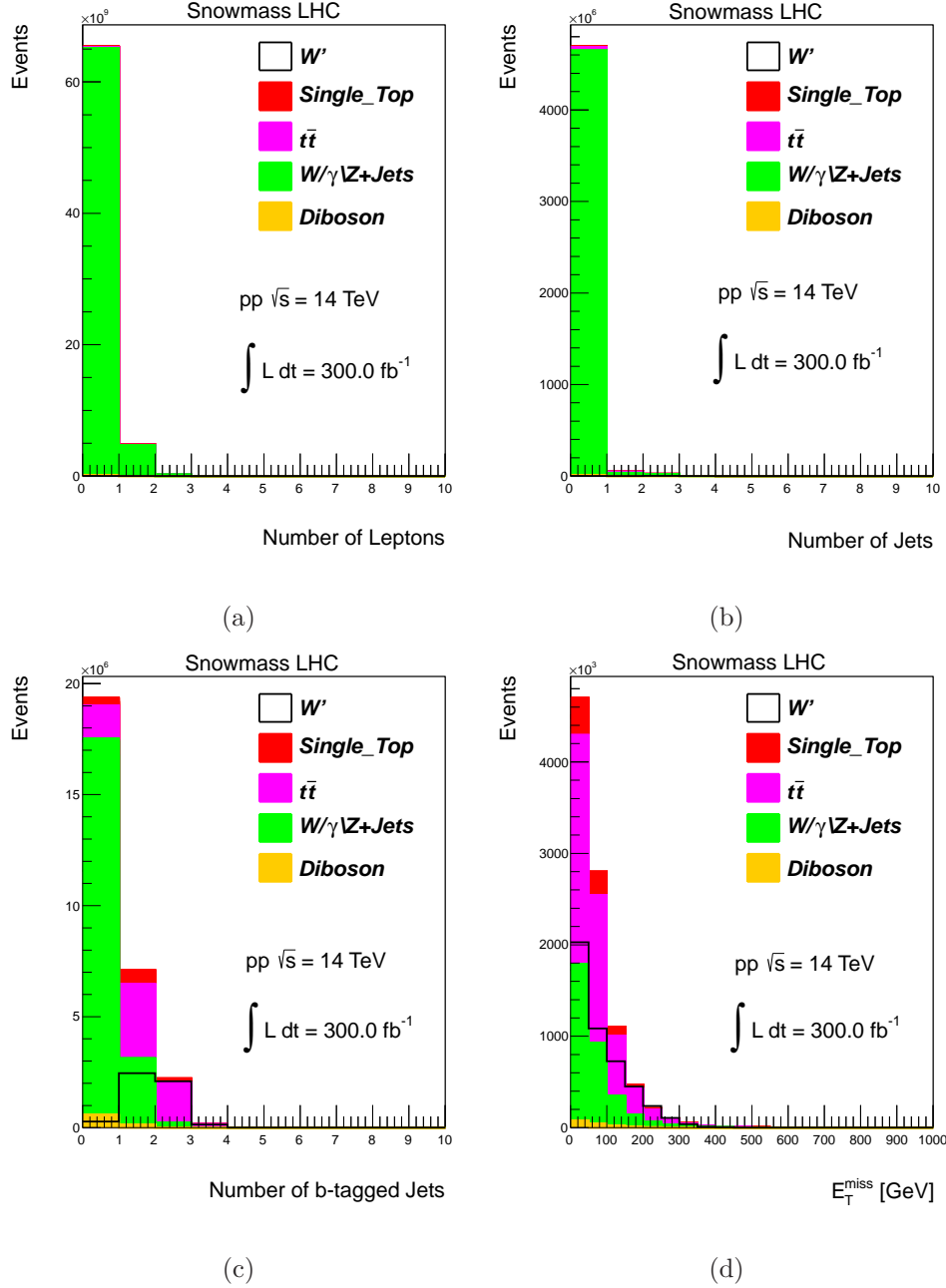


FIG. 3: Some kinematic distributions after all cuts leading up to the variable in question have been applied: (a) exactly one lepton, (b) at least two jets, (c) at least one  $b$ -tagged jet, and (d)  $E_T^{miss}$  requirement. The  $W'$  contribution corresponds with a generated mass of 1 TeV for  $300 \text{ fb}^{-1}$  at 14 TeV. This signal sample is scaled up by a factor of 10.

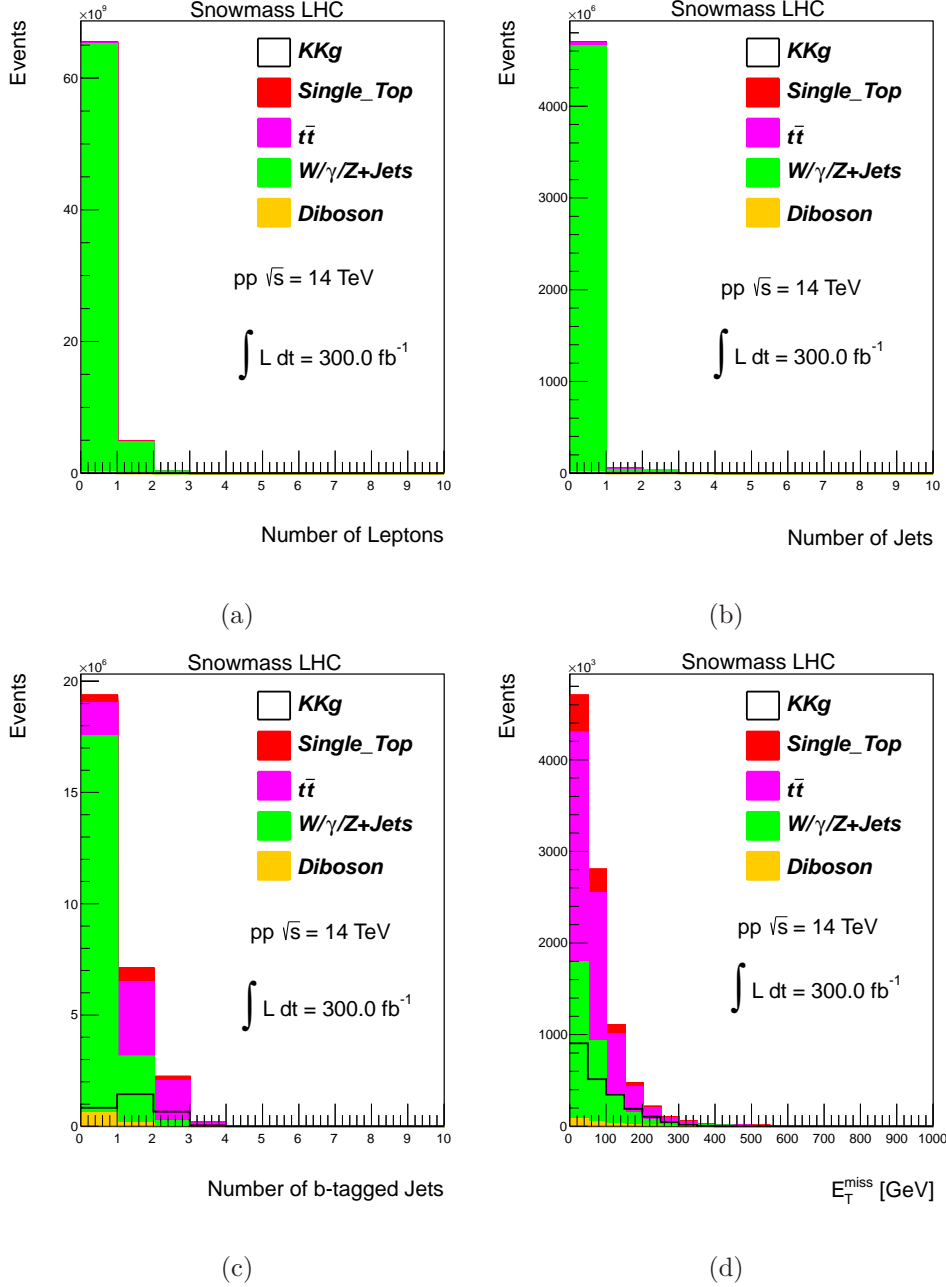


FIG. 4: Kinematic distributions after all cuts leading up to the variable in question have been applied: (a) exactly one lepton, (b) at least two jets, (c) at least one  $b$ -tagged jet, and (d)  $E_T^{miss}$  requirement. The  $KKg$  contribution corresponds with a generated mass of 1 TeV for  $300 \text{ fb}^{-1}$  at 14 TeV. This signal sample is scaled up by a factor of 10.

68 **IV. EVENT SELECTION**

69 To improve the signal to background ratio, events are required to pass the following  
 70 additional selection cuts in the  $KKg$  analysis:

$$\begin{aligned}
 & \text{Lepton with } p_T^\ell \geq 100 \text{ GeV,} \\
 & \text{Jet with } p_T^j \geq 300 \text{ GeV,} \\
 & \text{Number of Subjets } \leq 2, \\
 & \text{Exactly 1 B-Tagged Jet,} \\
 & \text{Exactly 1 Non-B-Tagged Jet,} \\
 & \text{Top Mass } \leq 200 \text{ GeV,} \\
 & \text{Reconstructed } KKg \text{ Mass } \geq \text{Generated Value.}
 \end{aligned}
 \tag{3}$$

71 The cuts are chosen from a larger set of available variables and cuts through a systematic  
 72 approach. For each cut on a given variable, the integral of the signal over the square root  
 73 of the background is computed. In addition, since the event yields in this analysis are large,  
 74 the systematic uncertainty on the background (10%) is taken into account by defining the  
 75 figure of merit ( $F.O.M$ ) as

$$F.O.M = \frac{S}{\sqrt{B + (0.1 \cdot B)^2}},
 \tag{4}$$

76 where  $S$  ( $B$ ) is the number of expected signal (background) events passing the cut.

77 Figure 6 shows the kinematic distributions for these  $KKg$  analysis variables for events  
 78 that pass the preselection cuts (Eq. 1) and the cuts from Eq. 3 up to the variable in question.

79 Similar, though not identical, cuts are used for the  $W'$  analysis:

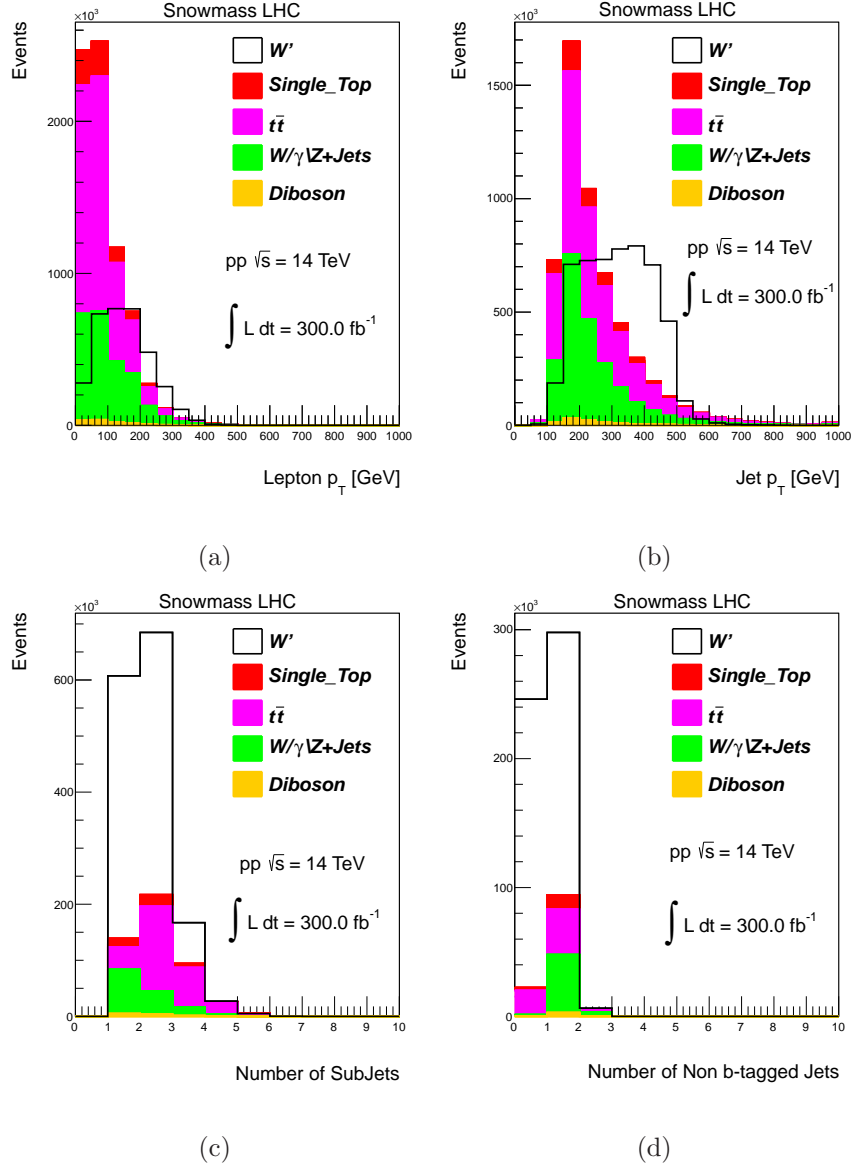


FIG. 5: Some kinematic distributions after all cuts leading up to the variable in question have been applied: (a) stricter lepton  $p_T$  cut, (b) stricter jet  $p_T$  cut, (c) number of subjets  $\leq 2$ , and (d) no non- $b$ -tagged jets. The  $W'$  contribution corresponds with a generated mass of 1 TeV for 300  $fb^{-1}$  at 14 TeV. This signal sample is scaled up by a factor of 10.

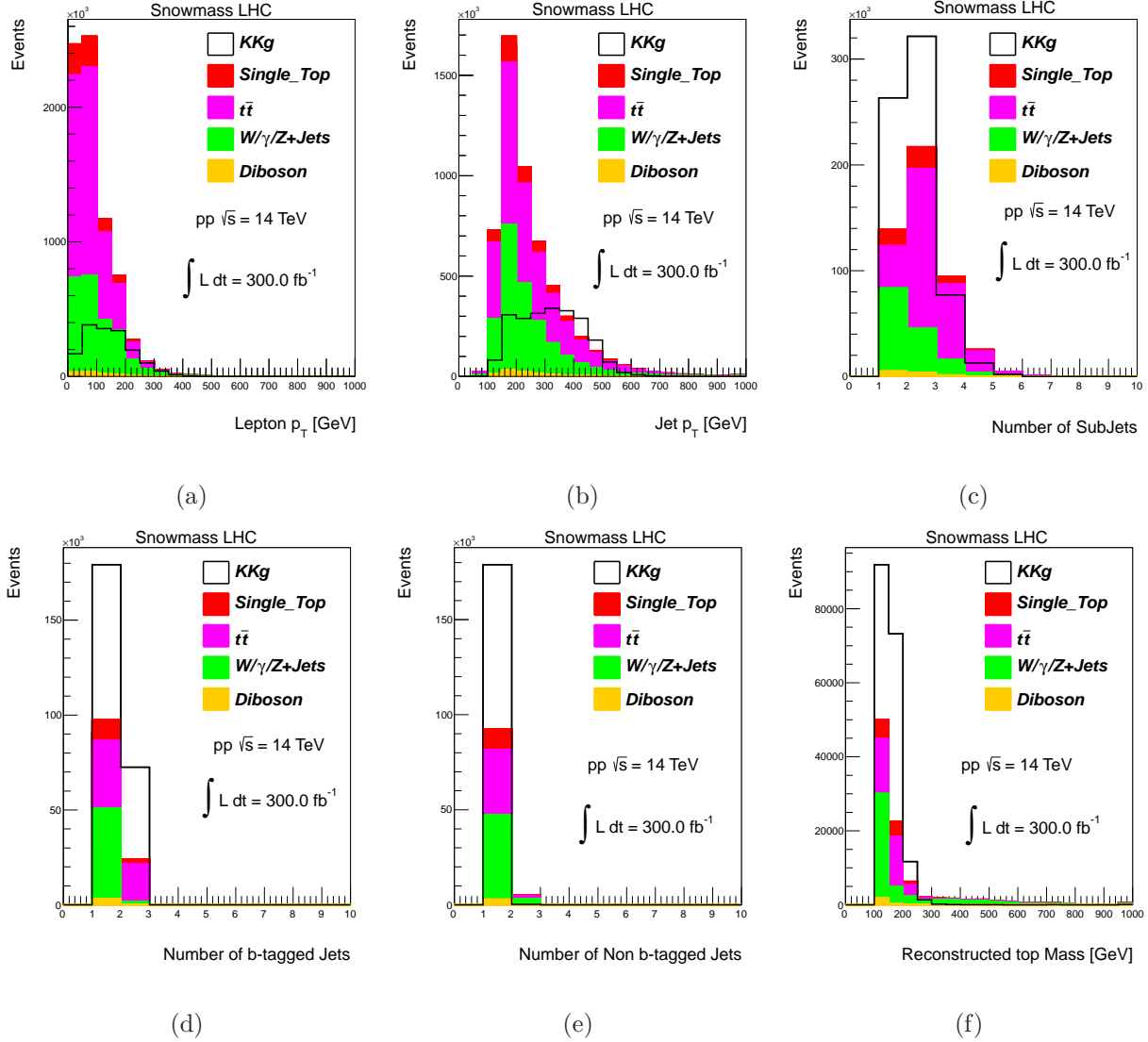


FIG. 6: Kinematic distributions after all cuts leading up to the variable in question have been applied: (a) lepton  $p_T$ , (b) jet  $p_T$ , (c) number of subjets  $\leq 2$ , (d) exactly one  $b$ -tagged jet, (e) exactly one non- $b$ -tagged jet, and (f) top mass. The  $KKg$  contribution corresponds with a generated mass of 1 TeV for 300  $fb^{-1}$  at 14 TeV. This signal sample is scaled up by a factor of 10.

$$\begin{aligned}
& \text{Lepton with } p_T^\ell \geq 100 \text{ GeV,} \\
& \text{All Jets with } p_T^j \geq 300 \text{ GeV,} \\
& \text{Number of Subjets } \leq 2, \\
& \text{Exactly 0 Non-B-Tagged Jets,} \\
& \text{Reconstructed } W' \text{ Mass } \geq \text{Generated Value.}
\end{aligned}
\tag{5}$$

80 Figure 5 shows the kinematic distributions for these  $W'$  analysis variables for events that  
81 pass the preselection cuts (Eq. 1) and the cuts from Eq. 5 up to the variable in question.

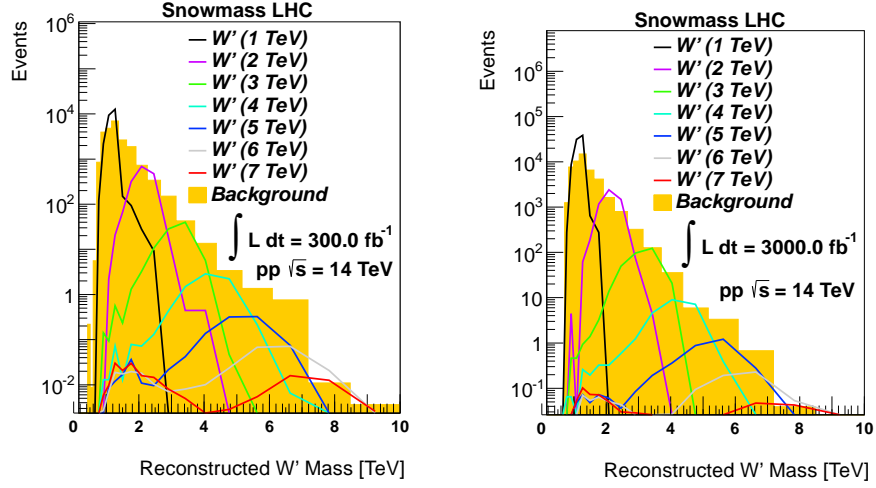
82 In each case, the neutrino is reconstructed from the  $E_T^{miss}$ ,  $E_T^{mis}$   $\phi$ , lepton  $p_T$ , lepton  
83  $\eta$ , and lepton  $\phi$  using a  $W$  boson mass constraint, which results in a quadratic equation  
84 that yields either one solution, two solutions, or imaginary solutions for the neutrino  $p_Z$ .  
85 In the case of two solutions, the smaller  $|p_Z|$  solution of the two is chosen. In the case  
86 of imaginary solutions, the neutrino  $p_T$  is scaled such that a solution is obtained with the  
87  $p_Z = 0$ . The  $W$  is reconstructed by adding the reconstructed neutrino to the lepton. The  
88 top is reconstructed using the reconstructed  $W$  and the jet that gives a top mass closest to  
89 172.0 GeV. The  $KKg$  and  $W'$  are both reconstructed using the reconstructed  $W$  and the  
90 two leading jets.

## 91 V. RESULTS

92 The reconstructed resonance mass for events passing the selection cuts are shown in Fig. 7  
93 for the  $W'$  analysis and in Fig. 8 for the  $KKg$  analysis.

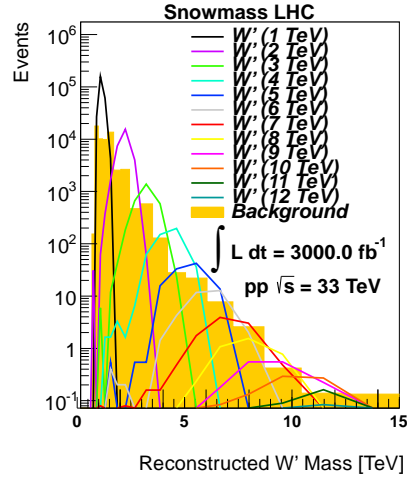
94





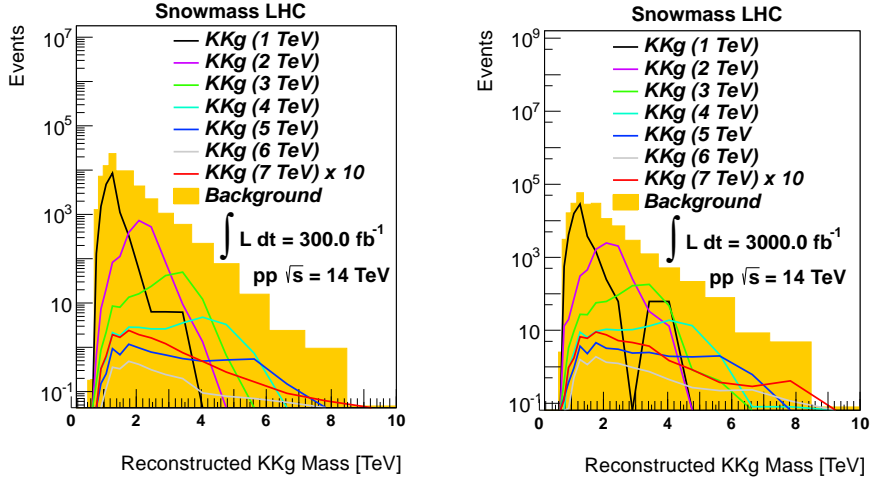
(a)

(b)



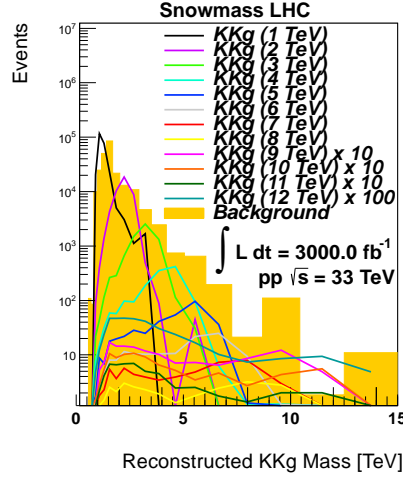
(c)

FIG. 7: The reconstructed  $W'$  masses: (a) at 14 TeV and  $300 \text{ fb}^{-1}$  luminosity, (b) at 14 TeV and  $3000 \text{ fb}^{-1}$  luminosity, (c) at 33 TeV and  $3000 \text{ fb}^{-1}$  luminosity.



(a)

(b)



(c)

FIG. 8: The reconstructed  $KKg$  mass: (a) at 14 TeV and  $300 \text{ fb}^{-1}$  luminosity, (b) at 14 TeV and  $3000 \text{ fb}^{-1}$  luminosity, (c) at 33 TeV and  $3000 \text{ fb}^{-1}$  luminosity.

95 Tables VII and VIII show the number of signal and background events passing the  
 96 final selection described above for the  $W'$  and  $KKg$  analyses, respectively, at various pileup  
 97 configurations, luminosities, and energies.

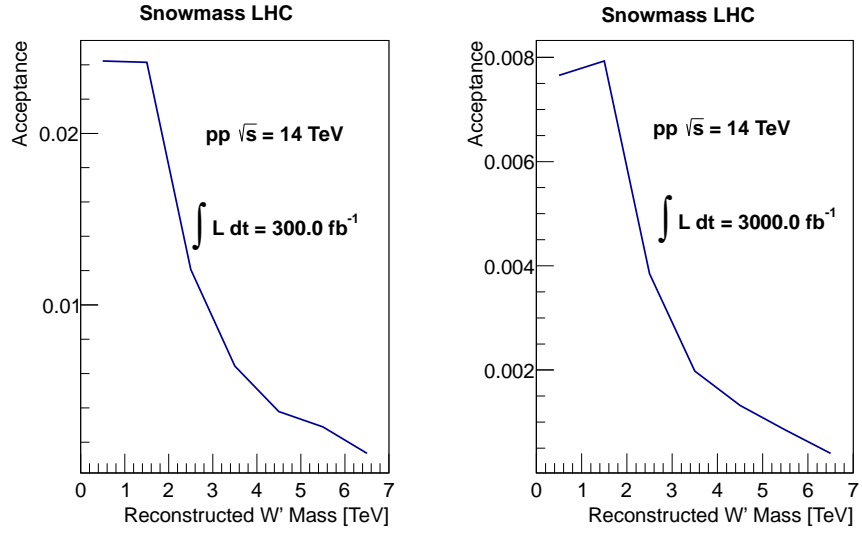
Final Selection	14 TeV		33 TeV
	300 $fb^{-1}$	3000 $fb^{-1}$	3000 $fb^{-1}$
$W'$ (1 TeV)	2.23E+04/1.76E+04	7.07E+04/3.89E+04	2.24E+05/4.02E+04
$W'$ (2 TeV)	1.07E+03/1.09E+03	3.50E+03/2.50E+03	1.95E+04/3.89E+03
$W'$ (3 TeV)	5.60E+01/8.46E+01	1.78E+02/2.19E+02	1.79E+03/6.92E+02
$W'$ (4 TeV)	4.19E+00/1.10E+01	1.29E+01/1.86E+01	2.85E+02/8.37E+01
$W'$ (5 TeV)	4.56E-01/2.36E+00	1.59E+00/4.29E+00	5.60E+01/3.31E+01
$W'$ (6 TeV)	9.69E-02/7.83E-01	2.85E-01/1.05E+00	1.48E+01/1.10E+01
$W'$ (7 TeV)	1.93E-02/2.20E-02	5.71E-02/3.92E-02	4.64E+00/5.00E+00
$W'$ (8 TeV)			1.79E+00/2.78E+00
$W'$ (9 TeV)			6.87E-01/6.95E-01
$W'$ (10 TeV)			3.70E-01/6.95E-01
$W'$ (11 TeV)			2.04E-01/2.73E-01
$W'$ (12 TeV)			8.55E-02/1.34E-01

TABLE VII: Signal and background event yields after the final selection for different integrated luminosities and CM energies for the  $W'$  analysis (represented as signal/total background).

Final Selection	14 TeV		33 TeV
	$300 \text{ fb}^{-1}$	$3000 \text{ fb}^{-1}$	$3000 \text{ fb}^{-1}$
$KKg$ (1 TeV)	1.49E+04/6.41E+04	5.01E+04/1.71E+05	2.26E+05/2.14E+05
$KKg$ (2 TeV)	1.21E+03/7.34E+03	4.43E+03/2.06E+04	2.80E+04/3.28E+04
$KKg$ (3 TeV)	7.69E+01/1.13E+03	2.81E+02/2.67E+03	3.61E+03/7.12E+03
$KKg$ (4 TeV)	6.84E+00/1.98E+02	2.67E+01/5.72E+02	6.29E+02/1.95E+03
$KKg$ (5 TeV)	7.93E-01/2.33E+01	3.04E+00/1.07E+02	1.35E+02/9.91E+02
$KKg$ (6 TeV)	7.88E-02/3.51E+00	3.49E-01/1.32E+01	3.56E+01/2.40E+02
$KKg$ (7 TeV)	9.12E-03/1.51E+00	4.98E-02/5.17E+00	1.28E+01/1.48E+02
$KKg$ (8 TeV)			4.74E+00/1.30E+02
$KKg$ (9 TeV)			1.43E+00/1.22E+02
$KKg$ (10 TeV)			7.16E-01/1.44E+01
$KKg$ (11 TeV)			2.40E-01/1.15E+01
$KKg$ (12 TeV)			6.52E-02/1.09E+01

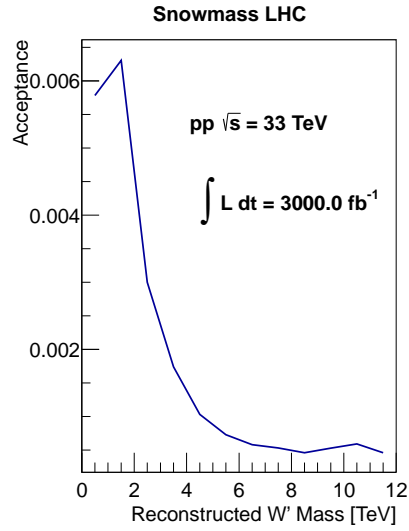
TABLE VIII: Signal and background event yields after the final selection for different integrated luminosities and CM energies for the  $KKg$  analysis (represented as signal/total background).

<sup>98</sup> We define the acceptance as the ratio of the initial number of events ( $W'$  or  $KKg$  events  
<sup>99</sup> including  $W$  decay to electron or muon) and the final number of selected events. The  
<sup>100</sup> acceptance for  $W'$  events to pass the selection cuts as a function of the  $W'$  mass is shown  
<sup>101</sup> in Fig. 9. The acceptance for  $KKg$  events to pass the selection cuts as a function of the  
<sup>102</sup>  $KKg$  mass is shown in Fig. 10.



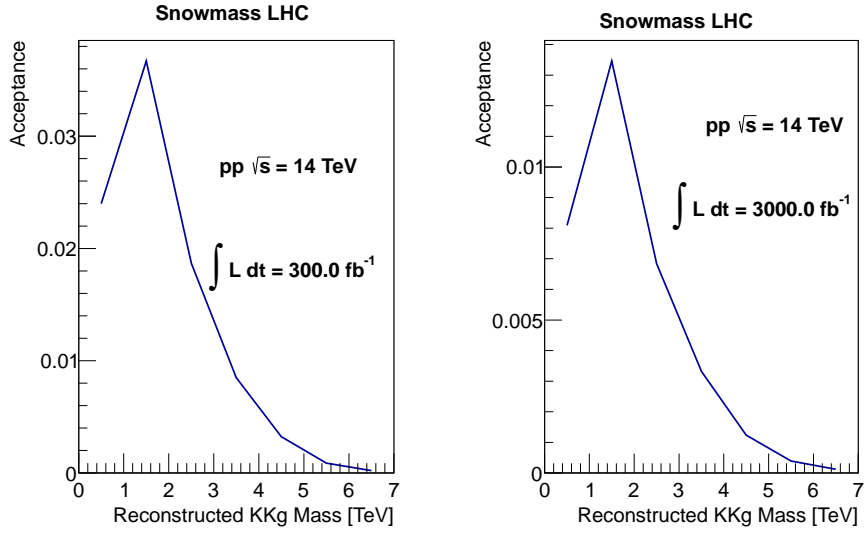
(a)

(b)



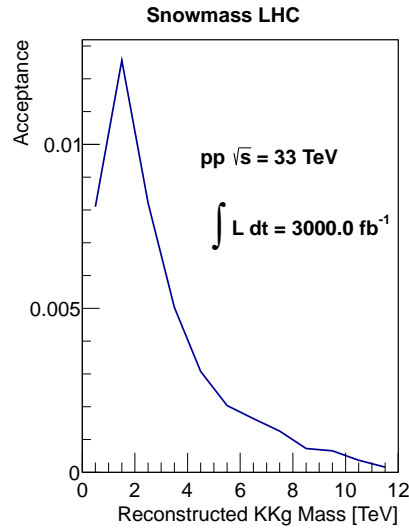
(c)

FIG. 9: The acceptance of the  $W'$  analysis at 14 TeV and  $300 \text{ fb}^{-1}$  luminosity (a), 14 TeV and  $3000 \text{ fb}^{-1}$  luminosity (b), and 33 TeV and  $3000 \text{ fb}^{-1}$  luminosity (c).



(a)

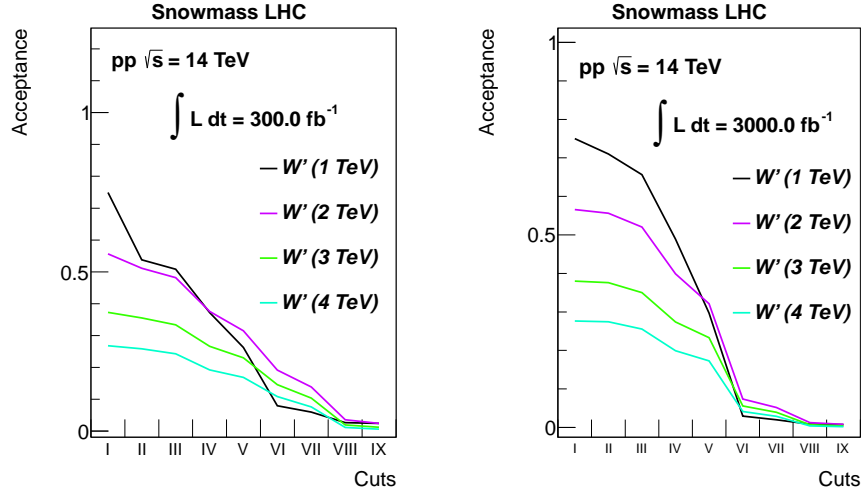
(b)



(c)

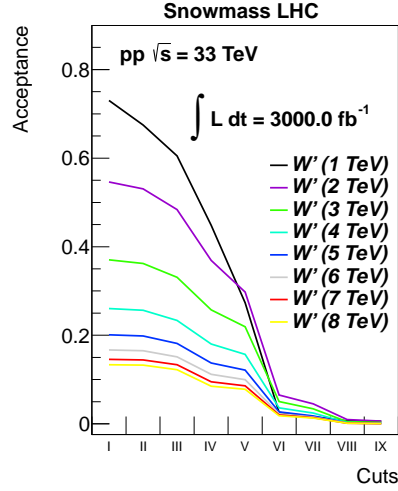
FIG. 10: The acceptance of the  $KKg$  analysis: (a) at 14 TeV and  $300 \text{ fb}^{-1}$  luminosity, (b) at 14 TeV and  $3000 \text{ fb}^{-1}$  luminosity, (c) at 33 TeV and  $3000 \text{ fb}^{-1}$  luminosity.

103 It is also interesting to view the acceptance as a function of the cut made, as for the  $W'$   
 104 analysis in Fig. 11 and for the  $KKg$  analysis in Fig. 12.



(a)

(b)



(c)

FIG. 11: The acceptance of the  $W'$  analysis by cut: (a) at 14 TeV and  $300 \text{ fb}^{-1}$  luminosity, (b) at 14 TeV and  $3000 \text{ fb}^{-1}$  luminosity, (c) at 33 TeV and  $3000 \text{ fb}^{-1}$  luminosity. The labeling of the cuts is as follows: I. Number of Leptons ( $= 1$ ), II. Number of Jets ( $\geq 2$ ), III. Number of  $b$ -tagged Jets ( $\geq 1$ ), IV.  $E_T^{miss}$  ( $\geq 25$  GeV), V. Lepton  $p_T$  ( $\geq 100$  GeV), VI. Jet  $p_T$  ( $\geq 300$  GeV), VII. Number of Subjets ( $\leq 2$ ), VIII. Number of non- $b$ -tagged Jets ( $= 0$ ), IX.  $W'$  Mass Window.

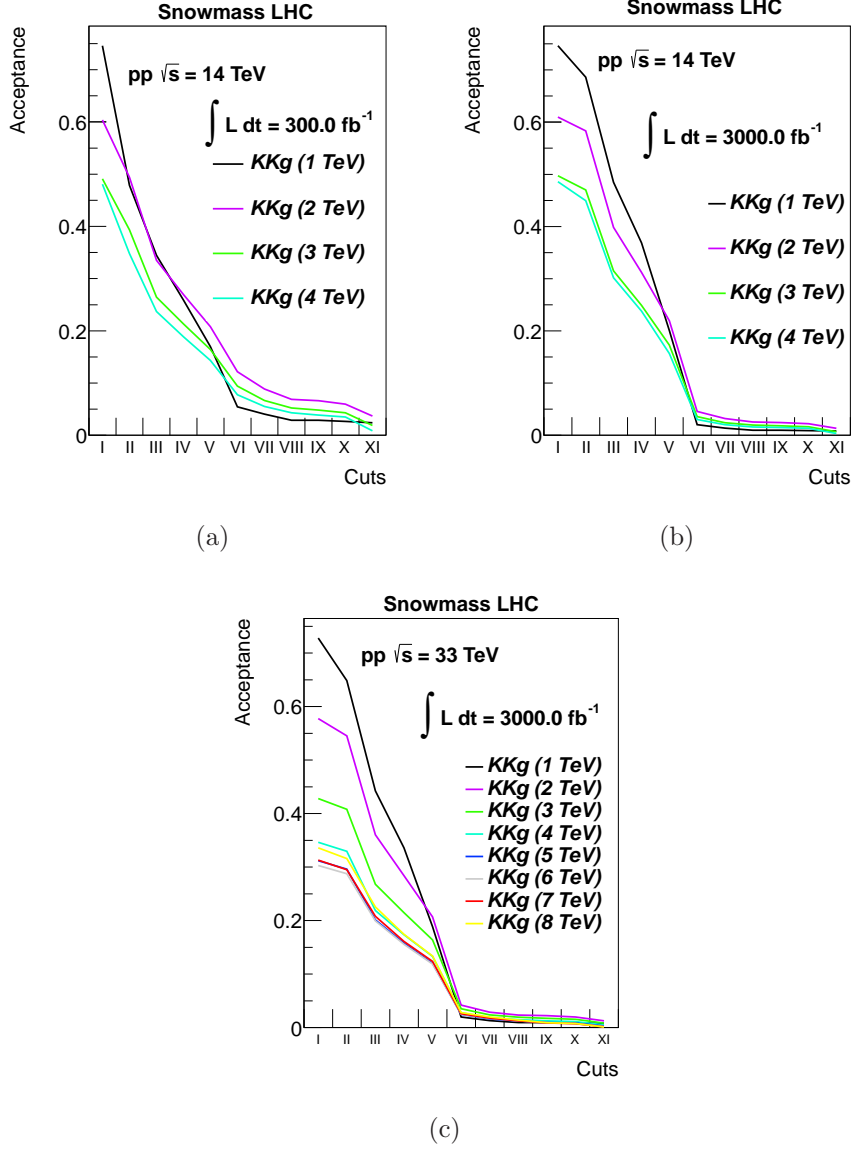


FIG. 12: The acceptance of the  $KKg$  analysis by cut: (a) at 14 TeV and  $300 \text{ fb}^{-1}$  luminosity, (b) at 14 TeV and  $3000 \text{ fb}^{-1}$  luminosity, (c) at 33 TeV and  $3000 \text{ fb}^{-1}$  luminosity. The labeling of the cuts is as follows: I. Number of Leptons ( $= 1$ ), II. Number of Jets ( $\geq 2$ ), III. Number of  $b$ -tagged Jets ( $\geq 1$ ), IV.  $E_T^{miss} (\geq 25 \text{ GeV})$ , V. Lepton  $p_T (\geq 100 \text{ GeV})$ , VI. Jet  $p_T (\geq 300 \text{ GeV})$ , VII. Number of Subjets ( $\leq 2$ ), VIII. Number of  $b$ -tagged Jets ( $= 1$ ), IX. Number of non- $b$ -tagged Jets ( $= 1$ ), X. Reconstructed top Mass ( $\leq 200 \text{ GeV}$ ), XI.  $KKg$  Mass Window.



## A. $W'$ Cross-Section Limits

106 Finally, 95% confidence limits on the  $W'$  and KKg cross-sections are set assuming a  
 107 background normalization uncertainty of 10%. The cross-section limits are converted into  
 108 mass limits using the theoretical dependence on the resonance mass.

109 Fig. 13 shows the cross-section times branching ratio as a function of the  $W'$  mass at  
 110 14 TeV and 33 TeV for different luminosities.

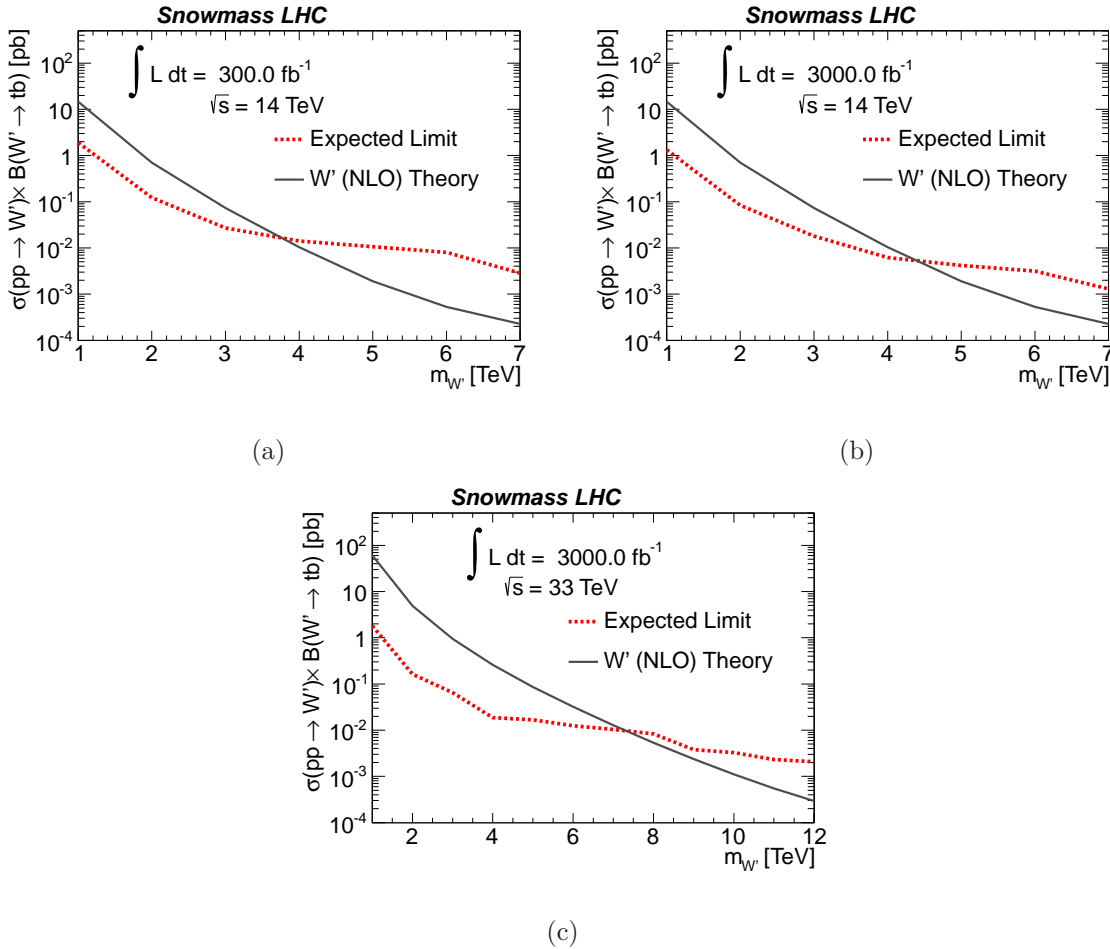


FIG. 13: The cross-section times branching ratio as a function of the  $W'$  mass: (a) at 14 TeV and  $300 \text{ fb}^{-1}$  luminosity, (b) at 14 TeV and  $3000 \text{ fb}^{-1}$  luminosity, (c) at 33 TeV and  $3000 \text{ fb}^{-1}$  luminosity.

111 The  $W'$  mass limit at 14 TeV is 3.8 TeV and 4.4 TeV for  $300 \text{ fb}^{-1}$  and  $3000 \text{ fb}^{-1}$   
 112 luminosity, respectively. The mass limit at 33 TeV and  $3000 \text{ fb}^{-1}$  luminosity is 7.3 TeV.  
 113 The expected  $W'$  cross-sections are show at Table IX.

$W'$ Mass [TeV]	14 TeV [pb]		33 TeV [pb]
	$300 fb^{-1}$	$3000 fb^{-1}$	$3000 fb^{-1}$
1 TeV	1.9E+00	1.3E+00	1.8E+00
2 TeV	1.2E-01	8.4E-02	1.6E-01
3 TeV	2.7E-02	1.8E-02	6.4E-02
4 TeV	1.4E-02	6.2E-03	1.9E-02
5 TeV	1.1E-02	4.2E-03	1.7E-02
6 TeV	8.0E-03	3.2E-03	1.3E-02
7 TeV	2.9E-03	1.3E-03	1.0E-02
8 TeV			8.3E-03
9 TeV			3.8E-03
10 TeV			3.3E-03
11 TeV			2.3E-03
12 TeV			2.1E-03

TABLE IX: Expected cross-section limits for various  $W'$  masses at 14 TeV and 33 TeV.

114 **B.  $KKg$  Cross-Section Limits**

115 Fig. 14 shows the cross-section times branching ratio as a function of the  $KKg$  mass at  
116 14 TeV and 33 TeV for different luminosities for the  $KKg$  analysis.

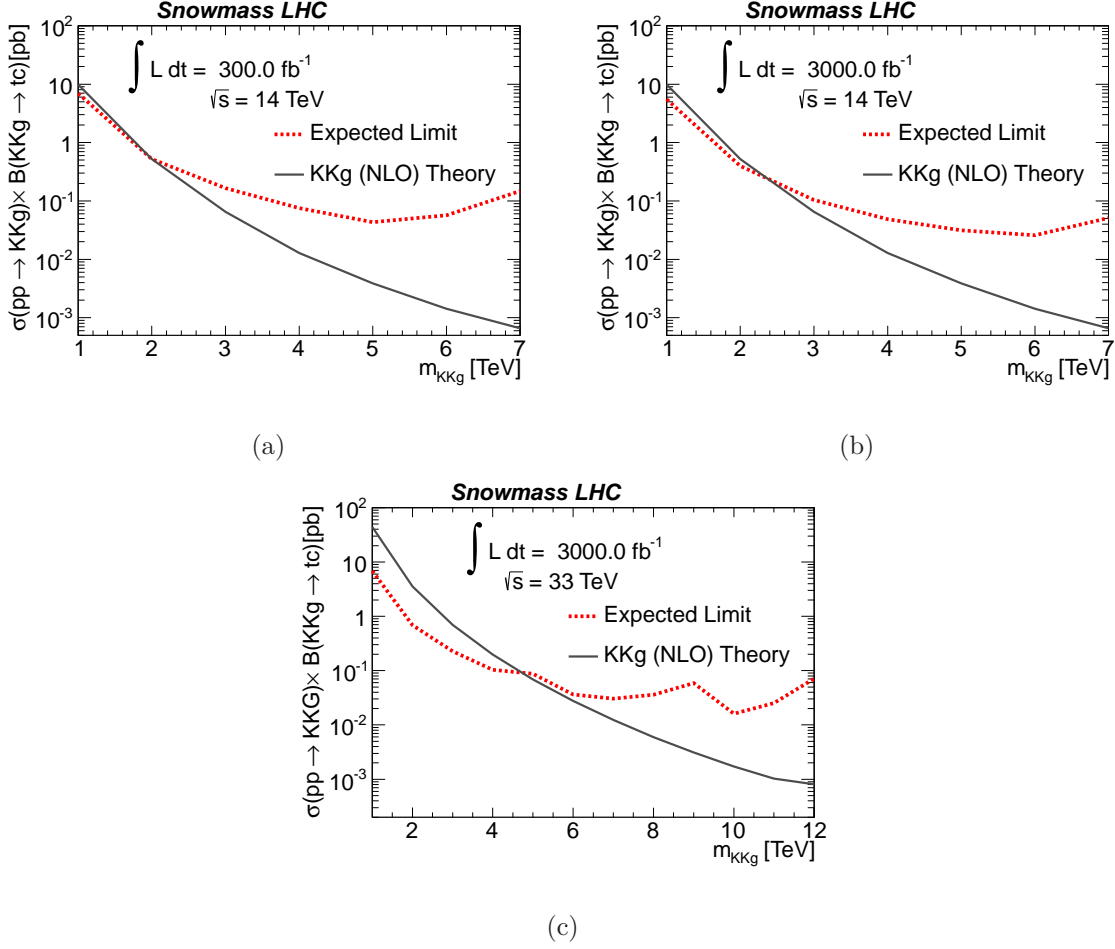


FIG. 14: The cross-section times branching ratio as a function of the  $KKg$  mass: (a) at 14 TeV and  $300 \text{ fb}^{-1}$  luminosity, (b) at 14 TeV and  $3000 \text{ fb}^{-1}$  luminosity, (c) at 33 TeV and  $3000 \text{ fb}^{-1}$  luminosity.

117 The  $KKg$  mass limit for at 14 TeV and  $300 \text{ fb}^{-1}$  luminosity is 2.0 TeV, at 14 TeV and  
 118  $3000 \text{ fb}^{-1}$  luminosity is 2.4 TeV, and 33 TeV and  $3000 \text{ fb}^{-1}$  luminosity is 4.7 TeV. The  
 119 expected  $KKg$  cross sections for the  $KKg$  analysis are show at Table X.

$KKg$ Mass [TeV]	14 TeV [pb]		33 TeV [pb]
	$300 \text{ fb}^{-1}$	$3000 \text{ fb}^{-1}$	$3000 \text{ fb}^{-1}$
1 TeV	7.0E+00	5.5E+00	6.9E+00
2 TeV	5.2E-01	4.0E-01	6.8E-01
3 TeV	1.7E-01	1.0E-01	2.3E-01
4 TeV	7.5E-02	4.9E-02	1.0E-01
5 TeV	4.3E-02	3.1E-02	8.8E-02
6 TeV	5.7E-02	2.6E-02	3.7E-02
7 TeV	1.5E-01	5.1E-02	3.0E-02
8 TeV			3.6E-02
9 TeV			5.6E-02
10 TeV			1.6E-02
11 TeV			2.5E-02
12 TeV			7.1E-02

TABLE X: Expected cross-section limits for various  $KKg$  masses at 14 TeV and 33 TeV for the  $KKg$  analysis.

## 120 VI. CONCLUSIONS

121 We have presented the possibilities for future searches for beyond the standard model  
122 particles at the LHC. The 14 TeV LHC is sensitive to  $W'$  bosons decaying to  $tb$  with right-  
123 handed couplings masses up to 3.8 TeV with  $300 \text{ fb}^{-1}$  and up to 4.0 TeV with  $300 \text{ fb}^{-1}$ . A  
124 33 TeV collider can reach  $W'$  masses up to 7 TeV. This will greatly improve the current  
125 limit of about 2 TeV set by ATLAS [6, 7] and CMS [8].

126 The sensitivity for FCNC  $KKg$  is not as good because the  $KKg \rightarrow tc$  final state only has  
127 one  $b$  quark, leading to large backgrounds. Only for a  $KKg \rightarrow tc$  cross section as large as  
128 40% of the  $KKg \rightarrow t\bar{t}$  NLO cross-section it will be possible to set limits, and even then only  
129 for  $KKg$  masses up to 2 TeV at the 14 TeV LHC. The situation is better at a 33 TeV hadron  
130 collider which has sensitivity up to 5 TeV for a  $KKg \rightarrow tc$  cross-section that is 40% of the  
131  $KKg \rightarrow t\bar{t}$  NLO cross-section. At low  $KKg$  masses, a 33 TeV hadron collider has sensitivity  
132 to  $KKg \rightarrow tc$  with a cross-section of about 5% of the  $KKg \rightarrow t\bar{t}$  NLO cross-section.

### 133 Acknowledgments

134 This work was supported in part by the U.S. National Science Foundation under Grants  
135 No. PHY-0952729 and PHY-1068318.

- 
- 136 [1] G. Aad et al. (ATLAS Collaboration), Phys.Lett. **B716**, 1 (2012), 1207.7214.  
137 [2] S. Chatrchyan et al. (CMS Collaboration), Phys.Lett. **B716**, 30 (2012), 1207.7235.  
138 [3] T. M. P. Tait and C. P. Yuan, Phys. Rev. D **63**, 014018 (2000), hep-ph/0007298.  
139 [4] A. Datta, P. O'Donnell, Z. Lin, X. Zhang, and T. Huang, Phys.Lett. **B483**, 203 (2000),  
140 hep-ph/0001059.  
141 [5] M. Perelstein, Prog.Part.Nucl.Phys. **58**, 247 (2007), hep-ph/0512128.  
142 [6] G. Aad et al. (ATLAS Collaboration), Phys.Rev.Lett. **109**, 081801 (2012), 1205.1016.  
143 [7] G. Aad et al. (ATLAS Collaboration), ATLAS-CONF-2013-050 (2013).  
144 [8] S. Chatrchyan et al. (CMS Collaboration), Phys.Rev.B. **718**, 1229 (2013), 1208.0956.  
145 [9] P. M. Aquino, G. Burdman, and O. J. Eboli, Phys.Rev.Lett. **98**, 131601 (2007), hep-  
146 ph/0612055.  
147 [10] C. Delaunay, O. Gedalia, S. J. Lee, G. Perez, and E. Ponton, Phys.Rev. **D83**, 115003 (2011),  
148 1007.0243.  
149 [11] K. Agashe, A. Belyaev, T. Krupovnickas, G. Perez, and J. Virzi, Phys. Rev. D. **77**, 015003  
150 (2006), 0612015.  
151 [12] R. S. Chivukula, A. Farzinnia, R. Foadi, and E. H. Simmons, Phys.Rev.D. **85**, 054005 (2011),  
152 1111.7261.

- 153 [13] J. Anderson, A. Avetisyan, R. Brock, S. Chekanov, T. Cohen, et al. (2013), 1309.1057.
- 154 [14] J. Alwall, M. Herquet, F. Maltoni, O. Mattelaer, and T. Stelzer, JHEP **1106**, 128 (2011),  
155 1106.0522.
- 156 [15] T. Sjöstrand et al., Computer Phys. Commun. **135**, 238 (2001), hep-ph/0010017.
- 157 [16] De Favereau J., Delaere C., Demin P., Giammanco A., Lematre V., Mertens A., Selvaggi M.  
158 (2013), 1307.6346.
- 159 [17] A. Avetisyan, J. M. Campbell, T. Cohen, N. Dhingra, J. Hirschauer, et al. (2013), 1308.1636.
- 160 [18] Z. Sullivan (2013), 1308.3797.
- 161 [19] A Cambridge-Aachen (C-A) based Jet Algorithm for boosted top-jet tagging,  
162 cds.cern.ch/record/1194489 (2009).
- 163 [20] M. Cacciari, G.P. Salam and G. Soyez, JHEP **04**, 63 (2008), arxiv:0802.1189.